The large amplitude oscillatory strain response of aqueous foam: Strain localization and full stress Fourier spectrum

Florence Rouyer[a], Sylvie Cohen-Addad[a], Reinhard Höhler[a], Peter Sollich[b], Suzanne Fielding[c]

[a] Université Paris-Est, Laboratoire de Physique des Matériaux Divisés et des Interfaces, UMR 8108 du CNRS, 5 Boulevard Descartes, 77 454 Marne-la-Vallée cedex 2, France

[b] King's College London, Department of Mathematics, Strand, London WC2R 2LS, U.K.

[c] Manchester Centre for Nonlinear Dynamics and School of Mathematics, University of Manchester, Manchester M13 9EP, U.K.

- Abstract -

We study the low frequency stress response of aqueous foams, subjected to oscillatory strain. As the strain amplitude is progressively increased starting from zero, the initially linear viscoelastic response becomes nonlinear as yielding sets in. To characterize this crossover from solid-like to liquid-like behaviour quantitatively, the full harmonic spectrum of the stress is measured. These results are compared to the soft glassy rheology model as well as to elastoplastic models. Moreover, to check for strain localization, we monitor the displacement profile of the bubbles at the free surface of the foam sample in a Couette cell using video microscopy. These observations indicate that strain localisation occurs close to the middle of the gap, but only at strain amplitudes well above the yield strain.

PACS. 83.80.Iz. (Foams and emulsions in Rheology) 47.57.Bc (Foams and emulsions in fluids dynamics) 83.60.La (Viscoplasticity, yield stress)

1. Introduction

Aqueous foam is a metastable disordered complex fluid, constituted of gas bubbles closely packed in a surfactant solution. It behaves like a viscoelastic solid or like a non Newtonian liquid, depending on gas volume fraction and applied stress [1-3]. In the work reported here, we focus on the nonlinear viscous, elastic and plastic response of 3D foams at the shear-induced transition between solid-like and liquid-like behaviour. Non Newtonian steady flow has been probed experimentally and interpreted in terms of interactions on the bubble scale [4-7]. Insight into the physical processes explaining the transient dynamics that accompany the *onset* of yielding requires additional experiments. Such information can be gained by applying oscillatory strain so that the sample switches back and forth between solid-like and liquid like behaviour on well defined scales of time and strain amplitude. Previous studies of the oscillatory foam response as a function of strain amplitude were focussed on the fundamental harmonic components of stress and strain [8,9] and discussed in terms of a strain amplitude dependent complex shear modulus. However, much additional information is contained in the spectrum of harmonics, or equivalently in the Lissajous representation showing the evolution of stress versus strain with the time as a parameter [10]. Indeed, for a fixed strain amplitude and frequency, the complex shear modulus alone does not allow to distinguish whether the dissipation of a predominantly elastic sample is of viscous or plastic origin. In contrast, a Lissajous plot does directly allow such a distinction since it exhibits a characteristic signature of the non linear response. It has the shape of an ellipse for viscous dissipation or of a parallelogram for plastic dissipation. Therefore, Lissajous data provide the opportunity to test physical foam rheology models predicting the onset of plastic response with increasing strain amplitude, corresponding on the local scale to the onset of strain induced irreversible bubble rearrangements. The evolution of the complex shear modulus with strain amplitude also provides information about the mechanisms involved in the sample deformation, but the following example shows that such evidence alone can be misleading. In a recent experimental study of a biological yield stress fluid

[11] the complex shear modulus was found to be almost independent of strain amplitude up to the yield strain so that one might have expected that the rheological response is linear in this entire range. Remarkably, a Lissajous plot revealed that this is not true: strong strain hardening is observed *within* each strain cycle. Motivated by this context, we study in the present paper the oscillatory response of 3D foam at the transition from solid-like to liquid-like behaviour, detecting for the first time the full stress harmonics spectrum.

Rheological studies of flowing foam, at a macroscopic scale, require great care, because the engineering strain, deduced from the relative motion of the sample boundaries, can be different from the local strain relevant for physical models, and it is possible that solid-like region and liquid-like region coexist in the same sample. This phenomenon is known as flow localization [7,12]. Since the conditions under which the flow of foam is localized are not yet clear [4,5,7,8,12-14], a reliable interpretation of engineering strain in terms of local strain requires in-situ observation of the sample deformation during the rheological experiment. We follow this approach and identify the limits of the range of strains where the flow is homogeneous.

The paper is organized as follows: In section 2.1, we first provide a brief overview of non linear rheological data for foams and concentrated emulsions. In section 2.2, we present theoretical models and we focus on those where in addition to conventional rheological characteristics, the full harmonics spectrum of the oscillatory stress response has been predicted. So far, the soft glassy rheology (SGR) model and a simple elasto-plastic model fulfil this criterion. Section 3 describes the sample preparation and the experimental procedures are given in sections 4 and 5. In section 6, experimental and theoretical results are compared and discussed in the framework of other recent experiments. On this basis, directions for further development of foam rheology models are pointed out.

2. Previous nonlinear rheological experiments and models

2.1. Experiments probing nonlinear rheology of 3D foams and concentrated emulsions

- *Experiments probing the solid-liquid transition.* Experimentally, the nonlinear rheological response of 3D foam at the transition from solid-like to liquid-like behaviour has been studied by measurements of the stress response to a steady applied shear rate [4-6,15], and to strain steps superimposed to such a constant strain rate [13]. These data alone do not fully characterize the nonlinear response: As the sample passes from solid-like to liquid-like behaviour, there is transient behaviour, evidenced by viscosity bifurcation dynamics [16] and the stress overshoot reported in shear start-up experiments [15]. Transient dynamics have also been probed by applying oscillatory strain [8,12,17]. At amplitudes far below the yield strain, the stress is sinusoidal and its amplitude scales linearly with strain amplitude. When the strain amplitude is increased nonlinear response such as shear induced normal stresses sets in [18]. Beyond the yield strain, there is a crossover of the real and imaginary parts of the complex shear modulus as a function of strain amplitude. This feature is often used as a criterion to determine the yield strain [8]. Moreover, oscillatory experiments probing how soft disordered materials yield as a function of strain rate amplitude have recently shown that frequency and strain amplitude dependence can be explained in terms of a structural relaxation time which depends on strain amplitude [9]. However none of these oscillatory experiments make use of the information contained in the harmonics spectrum of the stress response, which provides the signature of the physical processes involved in dissipation, as explained in the introduction.

- *Flow localization.* Flow localization of a yield stress fluid can occur as a direct consequence of stress heterogeneity. For example, if a steady torque is applied in a cylindrical Couette geometry, the stress increases with decreasing distance from the inner cylinder. If the stress remains larger than the yield stress only in the vicinity of this cylinder, localized flow sets in. Previous authors have ruled out other forms of localized foam flow because they obtained compatible results in

different rheological geometries [4,8]. Multiple light scattering studies of the flow profile in Couette experiments [4] and observation of the bubble motion at the free sample surface for samples obtained with a variety of foaming solutions in the plate-plate geometry [5] provided additional evidence in favour of this conclusion. However, other experiments with 3D foams have evidenced flow localization that cannot be interpreted as a direct consequence of stress heterogeneity. Coexistence of solid-like and flowing regions has been observed inside dry 3D foam undergoing steady planar shear start-up flow where the stress is homogeneous [14]. Moreover, MRI observations of the flow in the cylindrical Couette geometry have shown that steady flow is impossible below a critical strain rate $\dot{\gamma}_c$ [7]. This means that for an engineering strain rate smaller than $\dot{\gamma}_c$, part of the sample must remain solid-like whereas another part flows at a shear rate $\dot{\gamma}_c$. At strain rates $\dot{\gamma}$ larger than $\dot{\gamma}_c$, the stress was found to scale with $\dot{\gamma}$ following a power law. In oscillatory shear experiments, shear localization in the *middle* of the gap has been observed [12]. This is an unexpected form of flow localization because the stress is highest in the vicinity of the inner cylinder. Let us note that the flow of 2D foams has recently been studied by many authors, but we will not discuss this work in the present paper focussed on 3D foams.

The flow profile at the free surface of concentrated emulsions has been studied in steady shear experiments using a Couette cell [19]. For emulsions with dispersed volume fractions well above 0.7, localized flow is reported whereas in more dilute emulsions, the flow was found to be homogeneous [19]. In other recent steady flow experiments with emulsions, strain localization was found only in the presence of attractive interactions between the droplets [20].

2.2 Models for the rheology of soft disordered materials

Fluidity models are based on a scalar measure of the "degree of jamming" or structural relaxation time, coupled to the flow history of the material: Flow breaks up the jammed structure and reduces the viscosity. In contrast, aging re-establishes the jammed structure and enhances the viscosity [21-23]. The most detailed approach of this kind is based on a Maxwell equation

$\partial_t \sigma = -a\,\sigma + G\dot{\gamma}$ where the parameter a is the fluidity [22]. Aging and shear rejuvenation are expressed by a non-linear differential equation that describe the spatial and temporal evolution of a, as well as its coupling to stress and strain rate. This model predicts flow heterogeneities reminiscent of shear banding, but which are not intrinsic to the sample in the sense that they are dependent on the boundary conditions for the fluidity at the walls confining the sample.

The SGR Model - The soft glassy rheology (SGR) model is motivated by the strikingly similar rheology of foams, emulsions pastes and other close packings of small soft units, suggesting that a generic mechanism may be involved. The model explains the rheological behaviour in terms of the dynamics of mesoscopic elements [24,25]. They are chosen sufficiently large compared to the bubbles, grains or droplets so that the local packing structure is not resolved in detail and so that the local strain, stress and yield stress of an element are well defined quantities. At the same time, the mesoscopic length scale is chosen small enough to capture spatial variations of local strain, stress and yield stress. The SGR model uses a simple mean field coupling between mesoscopic and macroscopic stress and it describes interactions between mesoscopic regions in terms of an effective noise temperature, denoted x.

In more detail, the SGR model describes an ensemble of mesoscopic elements of the material, each of which is characterized by its local yield energy density E and strain l, the latter being measured relative to a local equilibrium configuration. Elements are assumed to deform elastically, with l incrementing in step with the global strain γ, until their local elastic energy reaches values of order E; they then yield stochastically. The elastic energy is taken to be of the simple quadratic form $kl^2/2$, with k a local elastic constant that is assumed to be uniform across the material for simplicity. The yield rate is the product of a microscopic inverse attempt time $1/\tau_0$, and an activation factor determined by the difference of the actual elastic energy to the yield value. After a yield, elements are taken to have zero local strain ($l=0$) relative to a new local equilibrium configuration, as well as a new yield energy drawn randomly from some fixed distribution $\rho(E)$. This distribution one presumes to be of exponential form,

$\rho(E) = (1/E_0)\exp(-E/E_0)$ for $E>0$. The mean E_0 of this is used to make the effective temperature parameter x dimensionless, i.e. the energy (density) available for activation is written as xE_0.

Mathematically, the above assumptions are summarized in the master equation for the probability $P(E,l,t)$ of a given element having yield energy E and strain l at time t:

$$\frac{\partial P}{\partial t} = -\dot{\gamma}(t)\frac{\partial P}{\partial l} - \frac{1}{\tau_0}\exp\left(-\frac{E - kl^2/2}{xE_0}\right)P + Y(t)\delta(l)\rho(E) \qquad (1)$$

The first term on the right corresponds to the uniform increment in the local strains of all elements that do not yield, according to $\dot{l} = \dot{\gamma}$. The second gives the decrease in probability due to yielding, and the third the corresponding increase in probability when elements are ``reborn'' after a yield; the factor $Y(t)$ can be found from the requirement of conservation of probability.

Once $P(E,l,t)$ has been determined, the global stress Σ is taken as the average of all local stresses kl across this distribution. It is possible, in fact, to solve for $P(E,l,t)$ analytically for a given strain history $\gamma(t)$, and this leads to two coupled constitutive integral equations for $\Sigma(t)$ and $Y(t)$ [24].

One can show that a glass (or jamming) transition takes place in the SGR model at $x=1$ [25, 26]. For smaller x and in the absence of steady shear, the system continues to evolve without ever reaching equilibrium: it ages. We will see, however, that the experimental data presented below can be reasonably fitted using values of x greater than unity. Consequently we will focus on the steady state predictions of the model. For oscillatory strain in particular, the amplitude and frequency dependent complex shear modulus $G^*(\Gamma_0,\omega)$ and the residual q (see Sec. 4 for definitions) can then be found by solving the constitutive equation numerically as outlined in Ref. [26].

We briefly discuss which parameters appear when fitting predictions of the SGR model to experimental data. The elastic (G') and viscous (G'') components of the complex modulus

$G^*=G'+iG''$ both scale with the local elastic constant k; this can be eliminated by normalizing by the linear response limit value (denoted G below) of G' at each given angular frequency ω. The dependence on frequency of the SGR predictions is through the dimensionless combination $\Omega=\omega\tau_0$. Similarly, the dependence on the strain amplitude Γ_0 is through a scaled strain Γ_0/Γ_{SGR}; the relevant scale is set by $\Gamma_{SGR}=\sqrt{E_0/k}$. The fitting procedure therefore involves finding optimal values for x, Ω and Γ_{SGR}. The result cannot be cast in any simple explicit form but examples of the variation of G^* with amplitude can be found in section 6.4 below.

Viscoelastoplastic models - Several constitutive laws [1,26-29], based on the association of springs, sliders and viscous elements, have been proposed to describe phenomenologically the homogeneous flow of complex yield strain fluids similar to foams. If the deformation is quasistatic, viscous effects vanish and elastoplastic behaviour is expected to be dominant. In this case, foam may be mimicked by a spring connected in series with a slider. The spring represents the static elastic response, characterized by a shear modulus G, whereas the slider schematically describes the yielding (cf. Figure 1a). It behaves as a rigid link when subjected to a force whose magnitude is below a threshold and it slides freely for forces of larger magnitude (cf. Figure 1b). In a material, the force and its threshold value respectively correspond to the stress Σ and the yield stress Σ_y where plastic flow sets in. To our knowledge, the first analytical prediction of the stress response to an oscillatory strain of an elastoplastic material is presented in [28]. The complex modulus and the stress harmonic spectrum are given in the appendix.

To introduce schematically viscoelastic behaviour at low strain amplitudes and to fit the yielding transition more accurately, an additional viscous element and a phenomenological yield function have been introduced [26,27]. A similar model has also recently been proposed in the context of complex polymeric fluids [30]. To summarize, these viscoelastoplastic models involving springs, sliders and viscous elements do not explain the physical mechanisms involved in foam rheology on the bubble or mesoscopic scale, but they have the merit of providing simple

constitutive laws where the information contained in experimental data is reduced to a relatively small number of parameters. However, they are restricted to flow regimes where strain localization does not occur.

3. Samples

We use stable foams for which drainage, coarsening and bubble coalescence are negligible over the duration of a rheological measurement. We study Gillette shaving cream which has been used in many rheological experiments published in the literature [2]. Its measured gas volume fraction is 92.5 ± 0.5 %. We also investigate a second kind of foam that will be called AOK. It is generated by injecting a gas and a polymer-surfactant-based aqueous solution into a column filled with glass beads, as described elsewhere [14]. This solution contains 1.5% g/g sodium α-olefin sulfonate (AOK, Witco Chemicals), 0.2% g/g Polyethylene-oxide ($M_w = 3 \times 10^5$ g mol^{-1}, Aldrich) and 0.4% g/g dodecanol (Aldrich). Its surface tension and viscosity are similar to those of the Gillette foaming solution. The gas is nitrogen containing perfluorohexane vapour. The measured gas volume fraction of the AOK foam samples is 97.0 ± 0.3 %. All experiments are performed at a temperature of 21 ± 1 °C. To mimimize the rheological memory of the flow history due to sample injection into the rheometer, Gillette samples are allowed to coarsen for either 30 or 60 minutes before the experiment is started. This leads to average bubble diameters equal to 28 μm and 36 μm respectively. For AOK foam, the experiments are done 20 minutes after sample injection when the average bubble diameter is 50 μm. Note that AOK foams coarsen much more slowly than Gillette foams.

4. Rheological experiments and data analysis

Immediately after its production, the foam is injected into the cylindrical Couette cell of a rheometer (Bohlin CVOR-150) with an inner radius $r_i = 21$ mm, an outer radius $r_o = 25$ mm and a rotor height H=48 mm. To prevent wall slip, closely spaced 0.2 mm deep grooves parallel to the

axis of the cylinders are carved into the surfaces in contact with the foam. The air in contact with the samples is saturated with humidity to avoid evaporation. When the sample has aged as described in the previous section, we apply a sinusoidal shear strain by rotating the inner cylinder. The frequency $\nu=\omega/2\pi$, is fixed either to 1 Hz or 0.3 Hz and the strain amplitude Γ_0 is increased from 10^{-3} to 3. This sweep is divided into steps where the amplitude is constant, lasting 5 seconds for 1 Hz and 10 seconds for 0.3 Hz. The rheometer is operating in a controlled strain mode. During the experiment it records as a function of time the engineering strain $\Gamma(t)= \Gamma_0 Re[exp(-i\omega t)]$ which is deduced from the angle of rotation of the inner cylinder $\theta(t)$ as :

$$\Gamma(t) = \frac{8 r_i^2 r_o^2 \theta(t)}{\left(r_i + r_o\right)^3 \left(r_i - r_o\right)} \tag{2}$$

Note that for linear elastic or Newtonian materials, this macroscopic quantity is equal to the strain in the middle of the gap. The rheometer also records the shear stress in the middle of the gap $\Sigma(t)$ which is deduced from the torque $M(t)$ applied to the inner cylinder:

$$\Sigma(t) = \frac{2M(t)}{\pi H (r_o + r_i)^2} \tag{3}$$

To first order in $(r_o - r_i) / r_i$, this stress is equal to the spatially averaged stress in the sample, and in the following, we will neglect the distinction between these two stresses. To analyze the stress data, we decompose them as follows:

$$\Sigma\left(t\right) = \Gamma_0 \,\mathrm{Re}\left[G^*\left(\Gamma_0, \omega\right) e^{i\omega t} \right] + \Delta\Sigma\left(t\right) \tag{4}$$

The first term is the fundamental harmonic component. It is related to the applied strain via $G^*\left(\Gamma_0, \omega\right)$, defined as the ratio of the fundamental harmonic components of shear stress and strain. Note that in the limit of small strain amplitude $G^*\left(\Gamma_0, \omega\right)$ does not depend on Γ_0 and converges to the usual linear complex shear modulus. The second term in Eq.(4), $\Delta\Sigma\left(t\right)$, contains the contributions of all the higher stress harmonics:

$$\Delta\Sigma(t) = \sum_{n=2}^{\infty} h_n \cos(n\omega t + \varphi_n) \tag{5}$$

where

$$h_n = \frac{\pi}{\omega}\left| \int_0^{2\pi/\omega} e^{-in\omega t}\, \Sigma(t)\, dt \right| \tag{6}$$

As shown in Figure 2 the third harmonic (n = 3) provides the dominant part of the nonlinear response, and contributions from harmonics where n is even or greater than 9 are found to be insignificant. To quantify the non linearity of the rheological response in a global way, we define the stress residual q as the dimensionless root-mean-square variation of $\Delta\Sigma(t)$:

$$q = \sqrt{\frac{\int \Delta\Sigma^2(t)\, dt}{\int \Sigma^2(t)\, dt}} = \sqrt{\frac{\sum_{i=1}^{4} {h_{2i+1}}^2}{{h_1}^2 + \sum_{i=1}^{4} {h_{2i+1}}^2}} \tag{7}$$

In our experiments, q is almost equal to the amplitude of the third harmonic. We nevertheless discuss our data in terms of q to provide a connection with the SGR model. We also analyse the Fourier spectrum of the recorded strain signal $\Gamma(t)$ which should ideally be perfectly sinusoidal. Its anharmonic residual, defined in analogy with q, is found to be smaller than 0.002. Therefore, we conclude that nonlinear stress response with q well above 0.002 is due only to the nonlinear rheological response of the foam.

5. Measurement of the local strain and stress

Before the shear experiment we draw a black radial line on the free foam surface between the two cylinders, using a suspension made of carbon black particles dispersed in the foaming solution. When oscillatory shear is applied by rotating the inner cylinder, the bubbles move to a good approximation on trajectories whose radial coordinate r is constant (cf. Figure 3). The black line is used as a tracer and we record its deformed shape as a function of time using a CCD camera. The curvilinear displacement of tracer points along their circular trajectories is observed

as a function of r and time t. For $r = r_i$, the bubbles move within experimental accuracy at the same velocity as the inner cylinder and at $r = r_o$ they are immobile. This observation excludes any wall slip.

We focus next on the *amplitude* of the bubble displacements during one oscillation period. The amplitude of the curvilinear bubble displacement at a radius r is denoted $s_0(r)$. The *local* shear strain amplitude $\gamma_0(r)$ is extracted from this function by the following expression, applied for a closely spaced set of radii, covering the range $r_i < r < r_o$:

$$\gamma_0(r) = \frac{\partial s_0(r)}{\partial r} - \frac{s_0(r)}{r} \tag{8}$$

The derivative in this expression is evaluated approximately by constructing a tangent to the experimental $s_0(r)$ curve. Due to the imperfection of the tracer, this construction is not accurate for r very close to either r_o or r_i and the corresponding points are omitted. The second term that is subtracted on the right hand side represents the change of s_0 with r expected for a rigid rotation without any strain.

Similarly, we can look at stress amplitudes, denoting Σ_0 and $\sigma_0(r)$ the amplitudes of the fundamental harmonic components of the shear stress $\Sigma(t)$ and of the local stress σ at a radius r. Since inertial forces acting on the foam are negligible in the investigated range of frequencies and strain amplitudes, and in view of Eq.(3) they are related as follows [31]:

$$\sigma_0(r) = \Sigma_0 \frac{(r_o + r_i)^2}{4r^2} \tag{9}$$

6. Results and discussion

6.1. Onset of strain localization - To monitor flow homogeneity we observe the bubble motion at the free surface of Gillette samples as described in section 5. As a reference, we calculate the displacement $s_0(r)$ for a Newtonian fluid or a linearly elastic solid. In both cases the displacement amplitude $s_0(r)$, normalized by the displacement amplitude of the rotor, $s_0(r_i)$ is predicted by:

$$\frac{s_0(r)}{s_0(r_i)} = Ar + \frac{B}{r} \tag{10}$$

where the constants A and B are chosen to fit the boundary conditions at r_i and r_o. Figure 4a compares Eq. (10) to the normalized displacement amplitudes measured for Gillette foam during a strain amplitude sweep. In view of the experimental uncertainty, the data for $\Gamma_0 = 0.3$ and 0.5 are in good agreement with Eq. (10). However, for the largest amplitude $\Gamma_0 = 0.7$ there are deviations larger than the error bar. These results are further analyzed in Figure 4b where the local strain amplitude $\gamma_0(r)$ is derived from the measured values of $s_0(r)$ using Eq (8). For a linearly elastic material or a Newtonian fluid, $\gamma_0(r)$ is expected to scale with $1/r^2$, as the stress. In our geometry, this implies $\gamma_0(r_i) \cong 1.20\ \Gamma_0$ and $\gamma_0(r_o) \cong 0.85\ \Gamma_0$, in rough agreement with our data for $\Gamma_0 = 0.3$ and 0.5. However, for $\Gamma_0 = 0.7$ the deformation has a maximum near the middle of the gap where the local strain reaches $2\ \Gamma_0$. This is the signature of strain localization, setting in above $\Gamma_0 = 0.6 \pm 0.1$ as reported previously [12]. Moreover, above a strain amplitude of 0.9 ± 0.1, we systematically observe a sharp discontinuity in the displacement profile, indicating strongly localized strain as shown in Figure 5. The picture is blurred close to the rotor because in this region the bubbles motion is faster than close to the stator. The quantitative analysis presented in Figure 4 was carried out only for one type of foam sample but qualitatively, strain localization *only close to the middle of the gap* for strain amplitudes larger than about 0.6 is observed for all of the investigated foams and frequencies. Since in cylindrical Couette geometry, the stress increases with decreasing distance from the axis the cylinders, localization would *a priori* be expected close to the inner cylinder as mentioned in section 2.1. Thus, we can exclude stress heterogeneity as the direct origin of the observed localization. Moreover, at least in simple shear and steady flow, the fluidity model outlined in section 2.2 predicts flow that is localized in the vicinity of boundaries, contrary to our observations.

These features demonstrate that for the foams investigated here, there exists a regime of localized oscillatory flow which is explained neither by stress heterogeneity, nor by fluidity

models. Our results also show that this localized flow only sets in at strain amplitudes well above the yield strain. As a consequence, there is a well defined regime where it is legitimate to compare our data to models of yielding that do not predict flow localization.

6.2. Local constitutive relation - We now use Eq. (8) and Eq. (9) to deduce from our observations the constitutive law relating local stress amplitude $\sigma_0(r)$ and strain amplitude $\gamma_0(r)$. In Figure 6, this relation is compared to the one between Σ_0 and Γ_0. Here stresses are normalized by the yield stress Σ_y which is determined as explained in section 6.3. For $\Gamma_0 < 0.6$, all the data are consistent, showing that in our case the continuum description of foam flow is indeed valid. This verification is necessary, since it has been suggested on the basis of previous MRI measurements of Gillette foams steadily flowing in a Couette geometry that in regions of the order of 25 bubble diameters, the continuum description can break down [7]. In our experiments this would correspond to a significant fraction of the gap.

At strain amplitudes Γ_0 larger than 0.6 there clearly are deviations between local and macroscopic rheological behaviours. Indeed, a narrow range of $\sigma_0(r)$ corresponds to a wide range of $\gamma_0(r)$. This local rheological behaviour confirms that the observed strain localization is not induced by the stress variation in the gap. Moreover, it is consistent with the coexistence of liquid-like and solid-like regions reported in [32]. This finding is robust with respect to changes of liquid volume fraction and bubble size in the investigated range.

6.3. Nonlinear rheological response – A typical Lissajous plot showing $\Gamma(t)$ versus $\Sigma(t)$ is shown in Figure 7a for a Gillette sample. The same qualitative behaviour is found for all investigated samples. At small amplitudes, the plot has an elliptic shape (Figure 7b), as expected for linear viscoelastic behaviour. With increasing strain amplitude, a cross over to a parallelogram shaped Lissajous plot is observed, as expected for elastoplastic materials (Figure 7b) (for further details see the appendix), and in qualitative agreement with Lissajous plots

predicted in the framework of the SGR models [24]. A variety of complex fluids showing similar behaviour have been classified in a phenomenological survey of large amplitude oscillatory strain responses [10]. These materials typically present a yield stress, and the flat and steep parts of the Lissajous diagram for large strain amplitudes correspond to liquid-like and solid-like response which alternately predominate during the oscillations. To analyze this behaviour quantitatively, we first focus on the fundamental frequency components of stress and strain from which we deduce the amplitude dependent complex shear modulus $G^*(\Gamma_0, \omega) = G'(\Gamma_0, \omega) + i\, G''(\Gamma_0, \omega)$ defined in Eq. (4). The insert of Figure 8a shows the typical evolution of $G'(\Gamma_0, \omega)$ with stress amplitude Σ_0. There is a linear regime at small Σ_0, characterized by a constant modulus that will be denoted G, and followed by the non linear regime where $G'(\Gamma_0, \omega)$ decreases following a power law. The intersection between these two asymptotic regimes is used to estimate the yield stress Σ_y as illustrated by the geometrical construction. Similar criteria have been used in many previous studies to detect yielding [8,10,19]. The criterion that we use here has been shown to be consistent with other methods for detecting the yield stress in 3D foams [12]. From this estimation, we derive the yield strain amplitude using the relation $\Sigma_y = |G^*(\Gamma_y, \omega)|\, \Gamma_y$. Within the studied range of frequency and bubble size, we obtain $\Gamma_y = 0.15 \pm 0.01$ for Gillette foam, and $\Gamma_y = 0.22 \pm 0.02$ for the AOK foam. Figure 8a and Figure 8b show the evolution of the elastic and loss moduli normalized by G as a function of the normalized strain amplitude Γ_0/Γ_y. We notice the evolution of G* with strain amplitude usually observed for foams: At small Γ_0 *a* solid-like regime where $G''(\Gamma_0, \omega) << G$, at large Γ_0 liquid-like behaviour with $G'(\Gamma_0, \omega) << G''(\Gamma_0, \omega)$ and a crossover between $G'(\Gamma_0, \omega)$ and $G''(\Gamma_0, \omega)$ close to the maximum of $G''(\Gamma_0, \omega)$. Our results are in qualitative agreement with previously reported data for moderately dry foams [8,12] and concentrated emulsions [33]. Let us recall that G scales as surface tension divided by mean bubble radius and that the complex shear modulus at low frequency scales as G. Therefore, the normalization by G allows variations in average bubble

size between different samples to be taken into account. For $\Gamma_0 < \Gamma_y$, only the normalized $G'(\Gamma_0, \omega)$ data are similar for all kinds of foams, whereas the normalized $G''(\Gamma_0, \omega)$ is smaller for AOK foam than for Gillette foam. This can be explained by the differences in gas volume fraction [8] and rate of coarsening induced bubble rearrangements [34,35]. For $\Gamma_0 > \Gamma_y$ the G^* data obtained at 1 Hz and 0.3 Hz with AOK foam and with Gillette foam for both investigated bubble sizes superimpose to a good approximation. Remarkably, at the strain amplitude where the onset of localized flow is observed, there are no distinctive features on the curves representing the G* data. Moreover, we notice that yielding and strain localization induced by oscillatory deformation are clearly distinct phenomena, since they set in at well separated strain amplitudes. This result is qualitatively consistent with previous observations of yielding and localization in steady shear start-up experiments with dry foam [14].

Finally, we plot in Figure 9 the anharmonic residual stress q defined in Eq. (7). For strain amplitude $\Gamma_0 << \Gamma_y$, the observed small level of anharmonicity is too close to the limit of detection to be interpreted quantitatively. However, for $\Gamma_0 \geq \Gamma_y$, q increases by more than one order of magnitude as the strain increases by a factor of 3. At amplitudes where strain localization sets in, the residual stress saturates. In contrast to the modulus $G^*(\Gamma_0, \omega)$ which is very similar for Gillette and AOK foam for $\Gamma_0 > \Gamma_y$, the respective stress residuals are clearly distinct: q rises much faster with strain amplitude for AOK foam compared to Gillette foam. We finally note that the stress residuals measured for an applied strain oscillation frequency of 1 Hz and 0.3 Hz are very similar. These latter findings strongly argue against artifacts related to the limited frequency bandwidth of the rheometer.

6.4 Comparison of our data with models – To introduce the discussion of specific models, we first recall recent measurements showing that the complex shear modulus of foams scales with strain amplitude and frequency as expected if a single structural relaxation time

dependent on strain rate amplitude, governed the stress relaxation and the rearrangement processes on the bubble scale. This relaxation time characterizes the dynamics globally, but it does not indicate how bubble rearrangement events are distributed in time *within* a strain cycle. This is a new feature that our harmonics (or Lissajous) data allow us to probe. An analogy with the Green Tobolsky model [36] well known in polymer rheology suggests that rearrangements that relax stress and that occur *randomly* in time would lead to Maxwell liquid behaviour. (Here, we make the simplifying assumption that foam elasticity in the absence of any rearrangements is linear). For a Maxwell liquid the Lissajous plot has an elliptical shape. This is approximately true for strain amplitudes up to the yield strain, but at higher amplitudes the plots clearly have a different shape, resembling a parallelogram. We find this behaviour up to the highest investigated strain amplitudes where we observe flow localization. The parallelogram shaped plot arises because rearrangements typically occur only if enough elastic energy has been built up locally. Our data contain the signature of this process, and therefore allow us to refine the physical description of the process of yielding. On this basis, we discuss in the following paragraphs the elastoplastic and SGR models. It would also be of great interest to compare our data to fluidity models, but this would require complex calculations which are beyond the scope of the present paper. A similar remark applies to models based on a minimal strain rate [23] which successfully describe steady foam flow. In their present form, they do not yet capture transient visco-elastic effects. Further theoretical work allowing additional models to be compared to our data would be of great interest.

Comparison with viscoelastoplastic models – For elementary elastoplastic behaviour, an analytical calculation first presented in [28] and recalled in the appendix predicts the stress response to oscillatory shear, given by Eq. (15). At strain amplitudes $\Gamma_0 >> \Gamma_y$, this result reduces to asymptotic power law decays:

$$G'(\Gamma_o,\omega)=\frac{16G}{3\pi}\left(\frac{\Gamma_0}{\Gamma_y}\right)^{-3/2} \tag{11}$$

and

$$G''(\Gamma_o,\omega)=\frac{4G}{\pi}\left(\frac{\Gamma_0}{\Gamma_y}\right)^{-1} \tag{12}$$

Note that the full analytic solution presented in the appendix shows that Eq. (11) is already reached at strain amplitudes close to Γ_y whereas the asymptotic power law for $G''(\Gamma_0, \omega)$ is reached only at strain amplitudes more than a decade larger than Γ_y. Figure 8a shows good agreement between Eq. (11) and the experimental data in the whole range of Γ_0/Γ_y. The prediction for $G''(\Gamma_0, \omega)$ given by Eq. (15) is in good agreement with the loss moduli data only for $\Gamma_0/\Gamma_y > 1$ (cf. Figure 8b). This is consistent with the fact that, for $\Gamma_0/\Gamma_y \ll 1$ the dissipation is mainly due to coarsening induced bubble rearrangements which are not taken into account by this elastoplastic model. Moreover, it is remarkable that the predictions of the elastoplastic model still hold in the regime where we observe a cross-over to localized flow. Here, one might identify the slider of the model with the region where the shear is localized and the spring with the part of the foam that may remain elastic.

The merit of the elastoplastic model is to predict the non linearity of $G^*(\Gamma_0, \omega)$ with strain amplitude using only two free parameters G and Γ_y whose physical origin on the scale of the microstructure is known [1]. The scaling of G with surface tension T and bubble radius R arises from the change of interfacial energy induced when the foam is sheared. Yielding in foams and emulsions is due to bubble or droplet rearrangements that arise when, under the effect of an applied strain, unstable configurations are created. Dimensionally, the yield stress also scales as T /R. The quantitative evolution of yield strain and elastic shear modulus with gas volume fraction has been described by phenomenological expressions [8].

Despite its success in describing the behaviour at large strain amplitudes, basic elastoplasticity remains an incomplete phenomenological model. It predicts a sharp transition from linear elastic behavior to plastic flow as a function of Γ_0. As a consequence, the predicted anharmonicity for strain amplitudes just above Γ_y is much larger than the measured data, as shown in Figure 9. A related weak discrepancy appears in the decay of *G'* with Γ_0 close to Γ_y. All these features suggest that a distribution of yield strains is necessary to describe the data more accurately. Marmottant et al have recently introduced a phenomenological yield function that describes such a distribution and which allows experimental complex shear modulus data to be fitted accurately [27]. Explicit predictions for the anharmonicity derived in this framework have not yet been published. Only if the same distribution of yield strains can be used to predict strain amplitude dependencies of both the stress Fourier spectrum and G^* close to Γ_y, is elastoplasticity a good concept for modelling foams accurately. A second shortcoming of the basic elastoplastic model is that it does not account for the dissipation experimentally observed for $\Gamma_0 << \Gamma_y$. To describe this feature, a viscous element connected in parallel to the plastic and elastic elements of the model has been proposed [27]. It allows the foam data to be fitted at a given frequency, but this model is not able to predict the experimentally observed $G^*(\Gamma_0)$ over an extended range of frequencies. Indeed, it reduces to a Voigt model in the linear viscoelastic regime, which is incompatible with the Maxwell liquid behaviour experimentally observed [13,34,37,38] at low frequencies and the power law increase $G^* \sim \omega^{1/2}$ found at high frequency [13,37,39].

- *Comparison with the SGR model*. For noise temperatures x close to 1, the SGR model predicts a strain amplitude dependence of the shear modulus similar to the experimental results shown in Figure 8. The ratio $G''(\Gamma_0, \omega)/G'(\Gamma_0, \omega)$ at low strain amplitude and low frequency is predicted to depend on *x* as follows:

$$\frac{G''(\Gamma_0,\omega)}{G'(\Gamma_0,\omega)} = \tan\left(\frac{\pi}{2}(x-1)\right) \tag{13}$$

We have $G''(\Gamma_0, \omega)/ G'(\Gamma_0, \omega) \cong 0.10$ for the Gillette foam for both bubble sizes and frequencies, and $G''(\Gamma_0, \omega)/ G'(\Gamma_0, \omega) \cong 0.055$ for AOK foam. Therefore, the relation (13) suggests $x \cong 1.07$ and $x \cong 1.05$ for the Gillette and AOK foams, respectively. These values then have to be tuned slightly to allow for the fact that the fitted (dimensionless) frequency Ω will not necessarily be small enough for Eq. (13) to apply exactly. In practice, we fit x and Ω to the data for G''/G, as this has the most structure in its dependence on strain amplitude Γ_0. This is done by minimizing the error in the predicted values for the maximum of G''/G and the height of the plateau in G''/G in the linear response regime of small Γ_0. The strain scale Γ_{SGR} is then fitted afterwards to reproduce the experimental value of the strain where the maximum of G''/G occurs.

The best fits obtained in this way are for x =1.08 (Gillette) and x =1.05 (AOK), close to the values expected from relation(13). Fits of similar quality can be obtained by varying x within the range ±0.01. The optimal associated values of the fitted frequency vary over a rather broad range, Ω=0.3±0.2 for both Gillette and AOK. Translating to the attempt frequency via $\Omega = 2\pi\nu\tau_0$ with ν = 0.3 Hz or 1 Hz one gets values of τ_0 in the range from 0.01s to 0.3s. As regards the strain scale, finally, $\Gamma_{SGR} = \Gamma_y$ is satisfactory for the Gillette foam, while for AOK the best fit value is slightly smaller at $\Gamma_{SGR} \approx 0.85\ \Gamma_y$. The fitted strain scale is therefore close to Γ_y as expected.

The SGR predictions using the parameter values given above are shown in Figures 7 and 8. For all foams and frequencies investigated, the predicted elastic modulus G'/G agrees with the experimental data for strain amplitudes up to Γ_0/Γ_y around 2, with deviations setting in at larger strain amplitudes. The predictions for the loss modulus G''/G agree quite well across the whole range of Γ_0 calculated. For the AOK foam, also the anharmonic residual q is predicted rather well by the model, while for the Gillette foam the onset of anharmonicity is predicted to be much

steeper than observed experimentally. The lower quality of the predictions for G'/G and q may in part be due to the fact that the SGR model cannot capture the observed onset of strain localization at large values of Γ_0/Γ_y, given that it treats elements from all areas of the sample as statistically indistinguishable. In addition, it is likely that the exponential form of the yield rate assumed in the model, cf. Eq. (1), becomes unrealistic for large strain amplitudes: Physically one expects that even elements which are strained beyond their yield barrier cannot yield arbitrarily quickly, so that the exponential increase of the yield rate with l^2 must be cut off eventually. One might expect that this would restore a somewhat more gradual decrease of G'/G, in line with experimental data, than predicted by the SGR model. Independently of these two shortcomings, why the model prediction for the anharmonicity q is so much more accurate for the AOK than for the Gillette foam remains unclear.

To explore the above suggestion further, we have investigated a modified SGR model where the exponential in Eq. (1) is replaced by unity when the exponent becomes positive, i.e. once an element has been strained past its notional yield point. Because the l-dependence then no longer appears as a simple factor, this model is not easy to study analytically, but can be simulated efficiently using waiting time Monte Carlo techniques [40]. At large strain amplitudes most SGR elements are pushed quickly into the regime where the cutoff on the yield rate kicks in, and one can show analytically that the predictions for $G^*(\omega)$ then become amplitude-independent and reduce to those of a Maxwell model with relaxation time τ_0.

To rectify this clearly unphysical behaviour, one can in addition postulate that the basic yield rate $1/\tau_0$ in Eq. (1) should increase with strain rate and be replaced by $1/\tau_0 + b\dot{\gamma}$ for some constant b, see e.g. [9,41]. The predictions of this version of the SGR model can still be worked out analytically in the limit of large strain amplitudes. Intriguingly, we find - and have confirmed by comparing with simulation results - that G' and G'' decay with strain amplitude according to the same power laws as in the elastoplastic model, see Eqs. (11)(12). This supports the view expressed above that such a modified SGR model should be capable of producing a good overall

fit to the experimental data. Because results at intermediate strain amplitudes currently have to be obtained by simulation we have not, however, attempted detailed fits of the relevant model parameters.

6.5 Connection with the foam microstructure and its dynamics. From a physicist's point of view, a complete model of foam rheology should explain how the macroscopic response arises due to processes on the scale of the bubbles and the liquid films. At this level of understanding it should be possible to predict all the free parameters of phenomenological models. In his pioneering work, Princen has provided insight about the dependence of the shear modulus and the yield stress on bubble size and average bubble size [1,2]. This is enough to predict the free parameters of a basic elastoplastic model to foam liquid fraction, surface tension of the foaming liquid and bubble size, or to fix the elastic constant of the mesoscopic regions and the scale of the distribution of trap depths in the SGR model. Providing a microscopic interpretation of the effective noise temperature x in the SGR model is more challenging. To discuss this point, we recall that quiescent coarsening foams have intrinsic, non-thermal dynamics due to the Laplace pressure driven diffusive gas exchange between neighbouring bubbles [1]. It induces intermittent structural rearrangements in small bubble clusters. One might therefore correlate the rate of coarsening to the effective noise temperature. Indeed, the Gillette foam that coarsens faster also has the higher noise temperature, according to the fits reported above. However, the rate of bubble rearrangements is known to be enhanced by steady flow [41], so that the noise temperature would have to depend on shear rate, a possibility which is not considered in the standard SGR model. Moreover, previous experiments and simulations have shown how coarsening induced rearrangements relax stress and lead on a macroscopic scale to Maxwell liquid behaviour in the low frequency limit [34,35,38]. A Maxwell liquid, mimicked by a spring in series with a viscous element, is characterized by a single characteristic time τ. As a consequence, G' progressively goes to zero for frequencies such that $\omega\tau < 1$, in agreement with

experimental data reported in [13]. The results of creep experiments are consistent with these findings [34]. In the SGR model a large spectrum of relaxation times is predicted and the experimentally observed very low frequency behaviour of the complex shear modulus is not found for x = 1.07. An additional feature not captured by the SGR model is the transient slowing down of bubble dynamics observed following a transient flow [17], which is the opposite of the shear rejuvenation effect observed in glasses.

7. Conclusion and outlook

The recent literature on liquid foam rheology raises the question whether the stress in a liquid foam is a well defined function of strain and strain rate, and, if so, how this constitutive law is related to physico-chemical processes and structures on a mesoscopic, bubble, or film scale. To answer the first question, we probe in situ the bubble displacement profile at the free sample surface of a Couette cell and show that strain localization clearly distinct from wall slip and not directly induced by heterogeneous stress is a robust feature of the investigated types of foams and oscillatory flows. Such behaviour is incompatible with conventional constitutive laws. However, localization only sets in at strain amplitudes far above the yield strain, demonstrating that there is indeed an extended regime of strains where it makes sense to compare the data to models.

This conclusion allows us to investigate the second question raised above, and we focus on a previously unexplored feature of the nonlinear rheological response. A variety of models of complex yield strain fluid rheology predict how the fundamental harmonic component of stress induced by an oscillatory strain depends on strain amplitude at low frequency. This information is generally represented in terms of the amplitude dependent complex shear modulus $G^*(\Gamma_0, \omega)$. To assess to what extent such models actually capture the relevant physics for foams, we measure and report for the first time in addition to $G^*(\Gamma_0,\omega)$ the full harmonic spectrum of the stress response of foam which can equivalently be represented in the form of a Lissajous plot.

These data resolve quantitatively how stress relaxation is distributed in time *within* a cycle of deformation, so that elastoplastic and viscoelastic behaviour with a strain rate dependent relaxation time can be distinguished. We find that this feature depends significantly on the physicochemical constitution of the sample, in contrast to the $G^*(\Gamma_0, \omega)$ data which do not show such a dependency in the vicinity of the yield strain.

For the driest investigated foam and at strain amplitudes well below the onset of flow localization, the SGR model accurately predicts the evolution with strain amplitude of three a priori independent functions, describing the nonlinear rheology: $G'(\Gamma_0,\omega)$, $G''(\Gamma_0,\omega)$ and the measure of the anharmonic response q. The fit is obtained with only two adjustable parameters (x, Ω). Phenomenological elastoplastic models capture the power law decay of the real and imaginary parts of the complex shear modulus in the liquid like regime. The two respective exponents are predicted correctly, without any free parameters. However, neither of the two mentioned approaches predicts the previously reported *frequency* dependence of the viscoelastic behaviour over an extended range [13,37,39] and accounts for the flow localization observed at high strain amplitudes. As a perspective for future work, it would be of great interest to construct a model of foam viscoelasticity and plasticity by combining the known facts about foam physics on the bubble scale with features of successful phenomenological models. We expect that the data reported in this paper will be useful in this context.

Acknowledgements

We acknowledge stimulating discussions with C. Gay, P. Marmottant and S. Cox and during the informal workshop on Foam mechanics, Grenoble, 21st - 27th January 2008. We thank D. Hautemayou for his technical help and we acknowledge financial support from E.S.A. (MAP AO99-108: C14914/02/NL/SH).

Appendix: Oscillatory response of an elastoplastic material

Figure 10 illustrates the basic elastoplastic response that can be mimicked by a combination in series of a spring and a slider (cf. Figure 1). Plastic strain and elastic strain respectively correspond to elongations of the slider and of the spring. The total strain Γ in the material that can be applied experimentally is given by the sum of its elastic and plastic components. Figure 10a illustrates the relation between shear stress Σ and strain Γ predicted for an ideal elastoplastic material subjected to the oscillatory strain shown in Figure 10b.

We now calculate the stationary response of such an elastoplastic element to an applied strain $\Gamma(t)= \Gamma_0 \cos(\omega t)$. If Γ_0 is smaller or equal to Γ_y, the response is purely elastic and $G^*(\Gamma_0, \omega) = G$. In this case, the stress oscillates sinusoidally with the same phase as the strain. If the strain amplitude is larger than Γ_y, the stress-strain relation becomes hysteretic, as shown in Figure 10b). As long as the slider is stuck, the plastic strain is constant so that any variation of the applied strain $\Delta\Gamma$ induces an equal change of the elastic strain and a stress variation $\Delta\Sigma = G \Delta\Gamma$. If the stress magnitude reaches the yield stress, the slider becomes mobile and any further increase of the applied strain magnitude induces only plastic strain while the elastic strain remains constant in this case.

As the applied strain decreases after having reached its maximum value, as for instance at $t = 0$ in Figure 10b, the slider becomes stuck. From here on, the evolution of the applied strain induces a decrease of the elastic strain equal to Γ_0-$\Gamma(t)$ and therefore a stress variation $\Sigma(t) = G \Gamma_y + G \Gamma_0 (\cos(\omega t) - 1)$. Indeed, this expression satisfies the initial condition at $t = 0$ as well as the relation $\Delta\Sigma = G \Delta\Gamma$ that must be valid as long as the slider is stuck. As time goes on, the stress decreases to $-\Sigma_y$ at a time denoted as t_1 (cf. Figure 10b). An elementary calculation yields:

$$t_1 = \frac{1}{\omega} \arccos(-2\Gamma_y / \Gamma_0 + 1) \qquad (14)$$

The stress then remains saturated until the minimum of the applied strain is reached at a time which is half the oscillation period T. As the strain starts increasing again, the elastic strain increases by $-\Gamma_0-\Gamma(t)$. Therefore the stress increases as $\Sigma(t) = - G\,\Gamma_y + G\,\Gamma_0\,(\cos(\omega t) + 1)$ until it reaches the value Σ_y, at the time $T/2 + t_1$. The evolution then remains saturated until the time t = T, and from then on the whole process continues periodically. To determine $G^*(\Gamma_0, \omega)$, we calculate the Fourier component of the stress oscillation at the frequency ω and divide it by the strain amplitude [28]. These expressions are simplified without any loss of generality by scaling stress and strain so that $G = 1$ and $\Gamma_y = 1$:

$$G^*(\Gamma_0,\omega)=\frac{2}{\Gamma_0 T}\left\{\int_0^{t_1}\left(1+\Gamma_0\left(\cos(\omega t)-1\right)\right)e^{-i\omega t}dt-\int_{t_1}^{T/2}e^{-i\omega t}dt+\int_{T/2}^{T/2+t_1}\left(-1+\Gamma_0\left(\cos(\omega t)+1\right)\right)e^{-i\omega t}dt+\int_{T/2+t_1}^{T}e^{-i\omega t}dt\right\}$$

$$=\frac{1}{\pi}\left(\arccos\left(\frac{-2+\Gamma_0}{\Gamma_0}\right)-\frac{2\left(-2+\Gamma_0\right)}{\Gamma_0}\sqrt{\frac{-1+\Gamma_0}{\Gamma_0^{\,2}}}+i\frac{4\left(\Gamma_0-1\right)}{\Gamma_0^{\,2}}\right) \qquad (15)$$

[1] D. Weaire and S. Hutzler, *The Physics of Foams*. (Oxford University Press, Oxford, 1999).
[2] R. Höhler and S. Cohen-Addad, Journal of Physics: Condensed Matter **17**, R1041 (2005).
[3] A. M. Kraynik, Ann. Rev. Fluid Mech **20**, 325 (1988).
[4] A. D. Gopal and D. J. Durian, Journal of Colloid and Interface Science **213** (1), 169 (1999).
[5] N. D. Denkov, V. Subramanian, D. Gurovich, and A. Lips, Colloids and Surfaces A **263** (1-3), 129 (2005).
[6] N. D. Denkov, S. Tcholakova, K. Golemanov, K. P. Ananthapadmanabhan, and A. Lips, Physical Review Letters **100** (13) (2008).
[7] S. Rodts, J. C. Baudez, and P. Coussot, Europhysics Letters **69** (4), 636 (2005).
[8] A. Saint-Jalmes and D. J. Durian, Journal of Rheology **43** (6), 1411 (1999).
[9] H. M. Wyss, K. Miyazaki, J. Mattsson, Z. Hu, D. R. Reichman, and D. A. Weitz, Physical Review Letters **98** (23) (2007).
[10] K. Hyun, S. H. Kim, K. H. Ahn, and S. J. Lee, Journal of Non-Newtonian Fluid Mechanics **107** (1-3), 51 (2002).
[11] R. H. Ewoldt, C. Clasen, A. E. Hosoi, and G. H. McKinley, Soft Matter **3** (5), 634 (2007).
[12] F. Rouyer, S. Cohen-Addad, and R. Hohler, Colloids and Surfaces A: Physicochemical and Engineering Aspects **263** (1-3), 111 (2005).
[13] A. D. Gopal and D. J. Durian, Physical Review Letters **91** (18), 188303 (2003).
[14] F. Rouyer, S. Cohen-Addad, M. Vignes-Adler, and R. Hohler, Physical Review E **67** (2), 021405 (2003).
[15] S. A. Khan, C. A. Schnepper, and R. C. Armstrong, Journal of Rheology **32** (1), 69 (1988).
[16] F. DaCruz, F. Chevoir, D. Bonn, and P. Coussot, Physical Review E **66** (5), 051305 (2002).
[17] S. Cohen-Addad and R. Höhler, Physical Review Letters **86** (20), 4700 (2001).
[18] V. Labiausse, R. Hohler, and S. Cohen-Addad, Journal of Rheology **51** (3), 479 (2007).
[19] T. G. Mason, J. Bibette, and D. A. Weitz, Journal of Colloid and Interface Science **179** (2), 439 (1996).
[20] L. Becu, S. Manneville, and A. Colin, Physical Review Letters **96** (13), 138302 (2006); L. Becu, P. Grondin, A. Colin, and S. Manneville, Colloids and Surfaces A: Physicochemical and Engineering Aspects **263** (1-3), 146 (2005).
[21] C. Derec, G. Ducouret, A. Ajdari, and F. Lequeux, Physical Review E **67** (6), 061403 (2003).
[22] G. Picard, A. Ajdari, L. Bocquet, and F. Lequeux, Physical Review E **66** (5), 051501 (2002).
[23] P. Coussot, Q. D. Nguyen, H. T. Huynh, and D. Bonn, Physical Review Letters **88** (17), 175501 (2002).
[24] P. Sollich, Physical Review E **58** (1), 738 (1998).
[25] P. Sollich, F. Lequeux, P. Hebraud, and M. E. Cates, Physical Review Letters **78** (10), 2020 (1997); M. E. Cates, in *Slow relaxations and nonequilibrium dynamics in condensed matter*, edited by M. F. J.L. Barrat, J. Kurchan, J. Dalibard (Springer, Berlin, 2002), Vol. LXXVII, pp. 74 ; M. E. Cates and P. Sollich, Journal of Rheology **48** (1), 193 (2004).
[26] P. Saramito, Journal of Non-Newtonian Fluid Mechanics **145** (1), 1 (2007).
[27] P. Marmottant and F. Graner, The European Physical Journal E - Soft Matter **23** (4), 337 (2007).
[28] V. Labiausse, Phd Thesis, Université de Marne-la-Vallée, 2004.
[29] S. Bénito, C. Bruneau, T. Colin, C. Gay, and F. Molino, The European Physical Journal E - Soft Matter **25** (3), 225 (2008).
[30] C. O. Klein, H. W. Spiess, A. Calin, C. Balan, and M. Wilhelm, Macromolecules **40** (12), 4250 (2007).
[31] C. Macosko, *Rheology, Principles, Measurements And Applications*. (Wiley-VCH, New York, 1994).
[32] P. Coussot, J. S. Raynaud, F. Bertrand, P. Moucheront, J. P. Guilbaud, H. T. Huynh, S. Jarny, and D. Lesueur, Physical Review Letters **88** (21), 218301 (2002).
[33] T. G. Mason, J. Bibette, and D. A. Weitz, Physical Review Letters **75** (10), 2051 (1995).
[34] S. Cohen-Addad, R. Höhler, and Y. Khidas, Physical Review Letters **93** (2), 028302 (2004).
[35] S. Vincent-Bonnieu, R. Höhler, and S. Cohen-Addad, Europhys. Lett. **74** (3), 533 (2006).
[36] R. Larson, *Constitutive Equations for Polymer Melts and Solutions*. (Butterworth-Heinemann, Boston, 1988).
[37] S. Cohen-Addad, H. Hoballah, and R. Höhler, Physical Review E **57** (6), 6897 (1998).
[38] S. P. L. Marze, A. Saint-Jalmes, and D. Langevin, Colloids and Surfaces A **263** (1-3), 121 (2005).
[39] A. J. Liu, S. Ramaswamy, T. G. Mason, H. Gang, and D. A. Weitz, Physical Review Letters **76** (16), 3017 (1996).
[40] A. B. Bortz, M. H. Kalos, and J. L. Lebowitz, Journal of Computational Physics **17** (1), 10 (1975).
[41] A. D. Gopal and D. J. Durian, Physical Review Letters **75** (13), 2610 (1995).

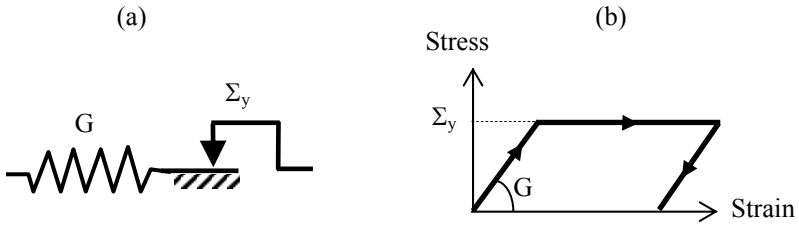

Figure 1 : (a) Schematic model of elastoplastic behaviour based on a spring and a slider, representing respectively an elastic modulus G and a yield stress Σ_y. **(b)** Stress-strain relationship of such an elastoplastic element.

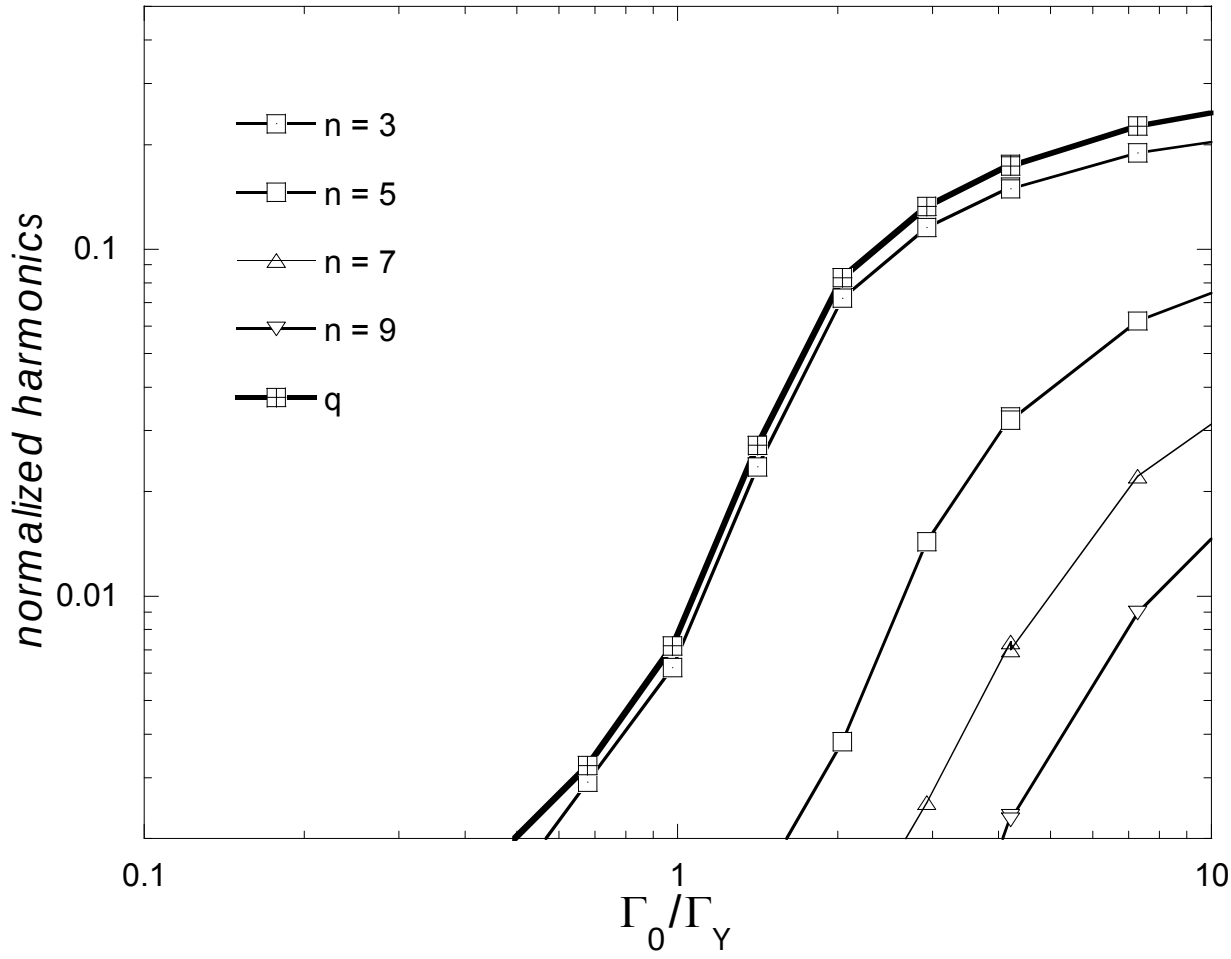

Figure 2 Stress residual *q* defined in Eq. **(7)** and odd harmonics from n =3 to 9 versus normalised strain amplitude, for AOK foam at 1Hz. The harmonics are normalized in the same way as the stress residual.

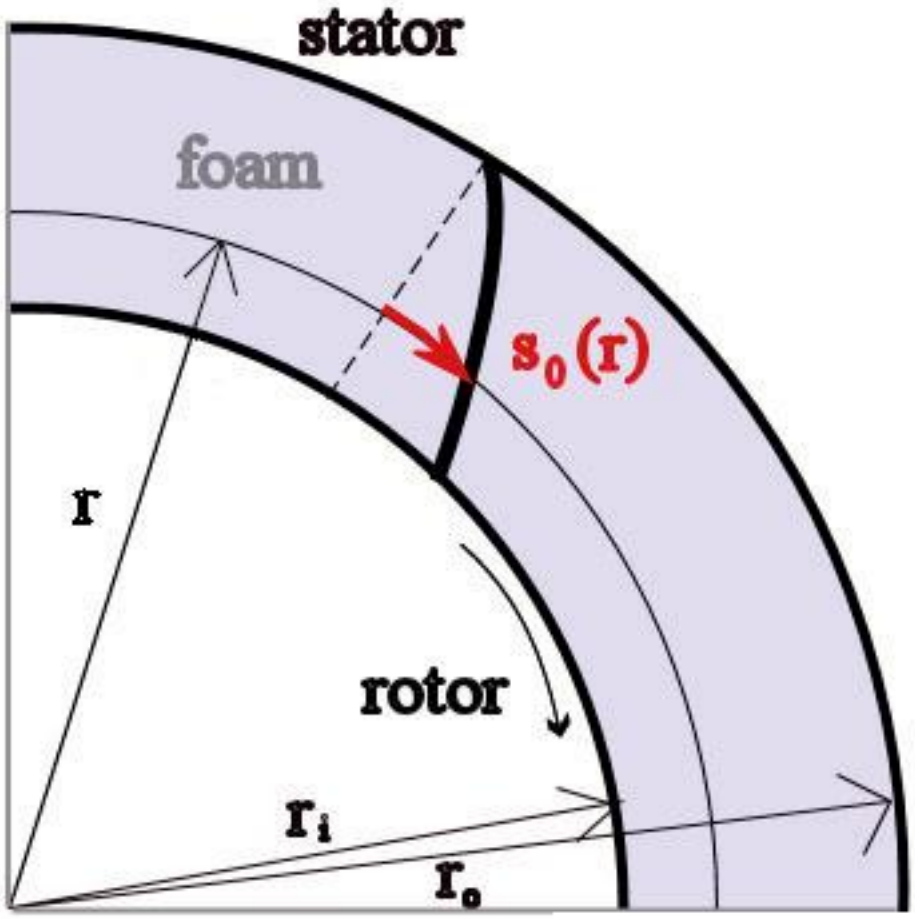

Figure 3 : Top view of the Couette cell illustrating the coordinates used in the analysis. The dashed line represents the tracer position before shear, and the continuous thick line shows its position after rotation of the inner cylinder. The thick arrow represents the amplitude of curvilinear tracer displacement $s_0(r)$, measured at a time t when $\Gamma(t)$ reaches its maximum value Γ_0.

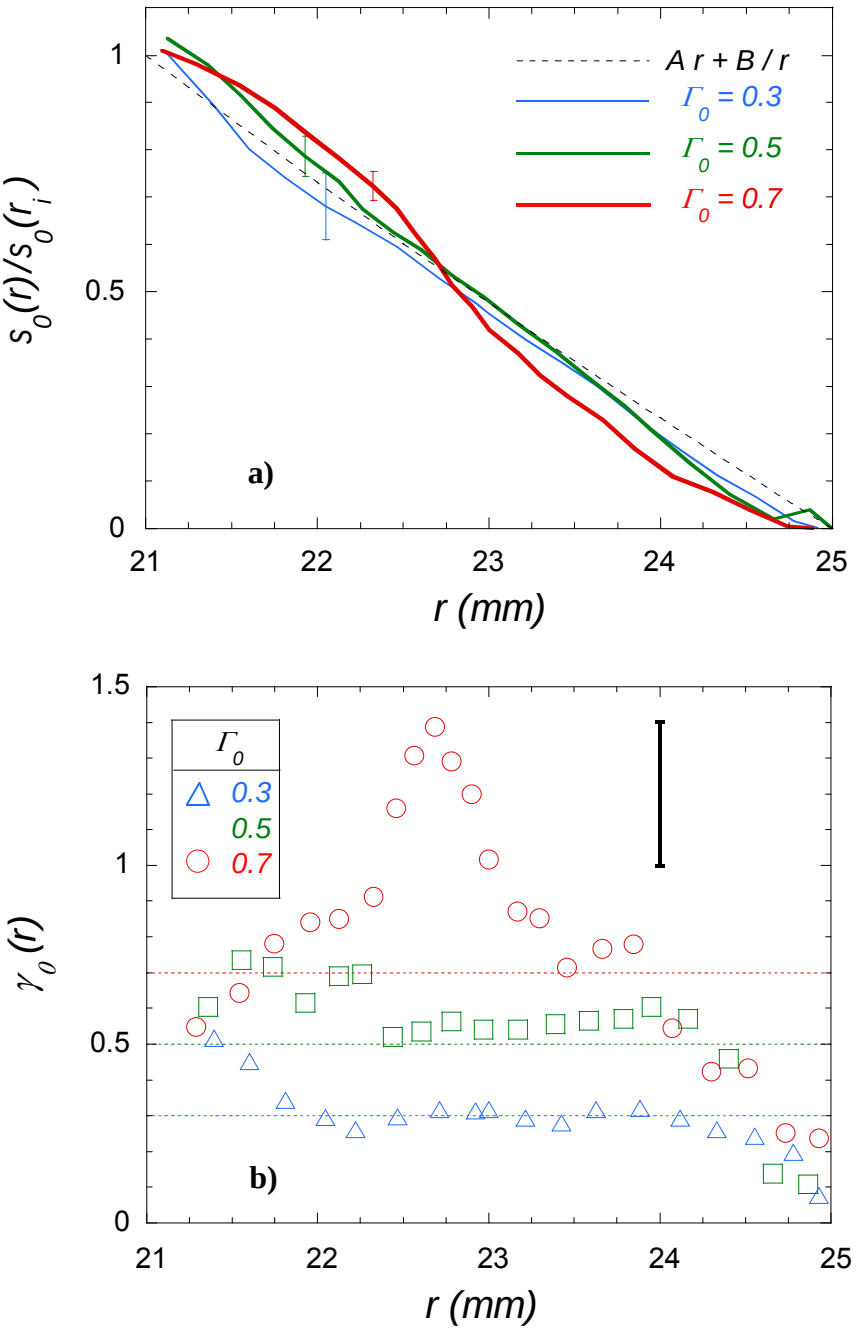

Figure 4: a) Normalized amplitude of the curvilinear displacement versus radial distance for increasing strain amplitudes Γ_0 applied to the same sample (Gillette foam, bubble diameter = 28 µm) at 1 Hz. The dashed line corresponds to the displacement expected for linear elastic deformation or Newtonian flow (Eq. (10) with A = - 0.11 mm^{-1} and B = 71 mm). Typical error bars are indicated. b) The local strain amplitudes derived from (a) using Eq.(8) are plotted versus the radial coordinate. The dotted lines correspond to the local amplitude expected in the middle of the gap for linear elastic deformation or Newtonian flow ($\gamma_0((r_i+r_o)/2) = \Gamma_0$).

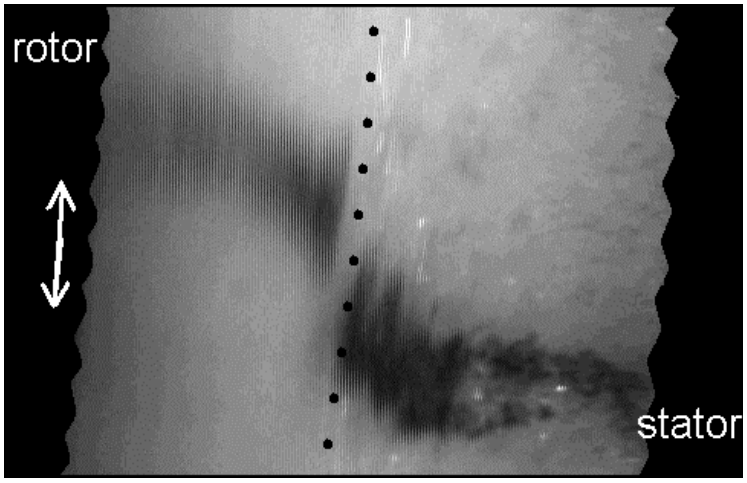

Figure 5 : Image of the free top surface of Gillette foam in the Couette cell. The applied strain amplitude Γ_0 is 0.9 and the picture is taken close to an instant where $\Gamma(t) \cong 0$. The rotor and the stator appear in black. A dotted line is drawn at the radius where the local strain is maximum.

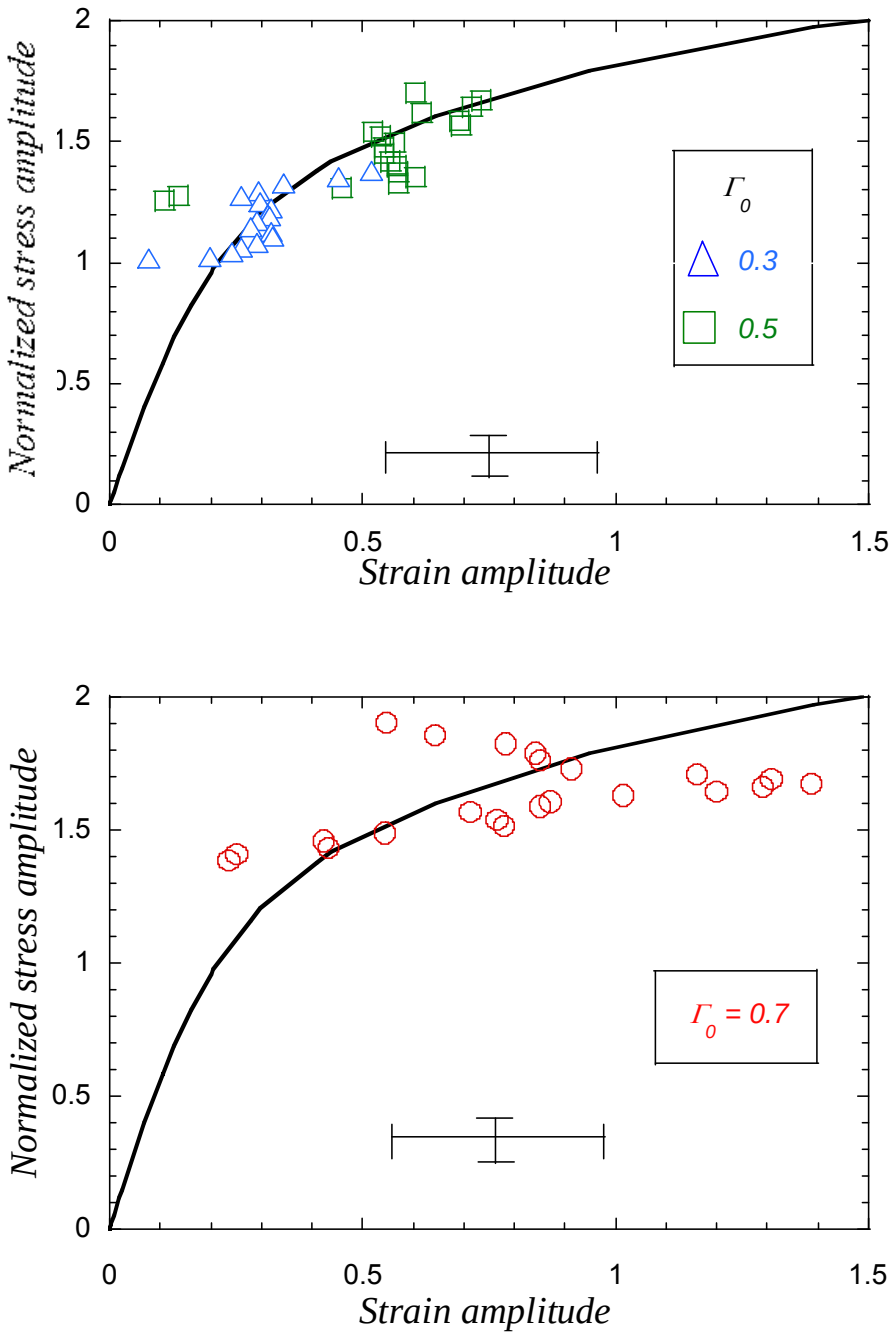

Figure 6 : Comparison of local and macroscopic normalised stress amplitudes versus strain amplitude. The lines correspond to the macroscopic stress amplitude Σ_0/Σ_y versus engineering strain amplitude Γ_0. The symbols represent the local stress amplitude normalized by the yield stress, $\sigma_0(r)/\Sigma_y$ versus local strain amplitude $\gamma_0(r)$. These data are deduced from **Figure 4**. Typical error bars for $\gamma_0(r)$ and $\sigma_0(r)/\Sigma_y$ are drawn. The sample is Gillette foam (average bubble size = 28 µm) and the frequency is 1 Hz.

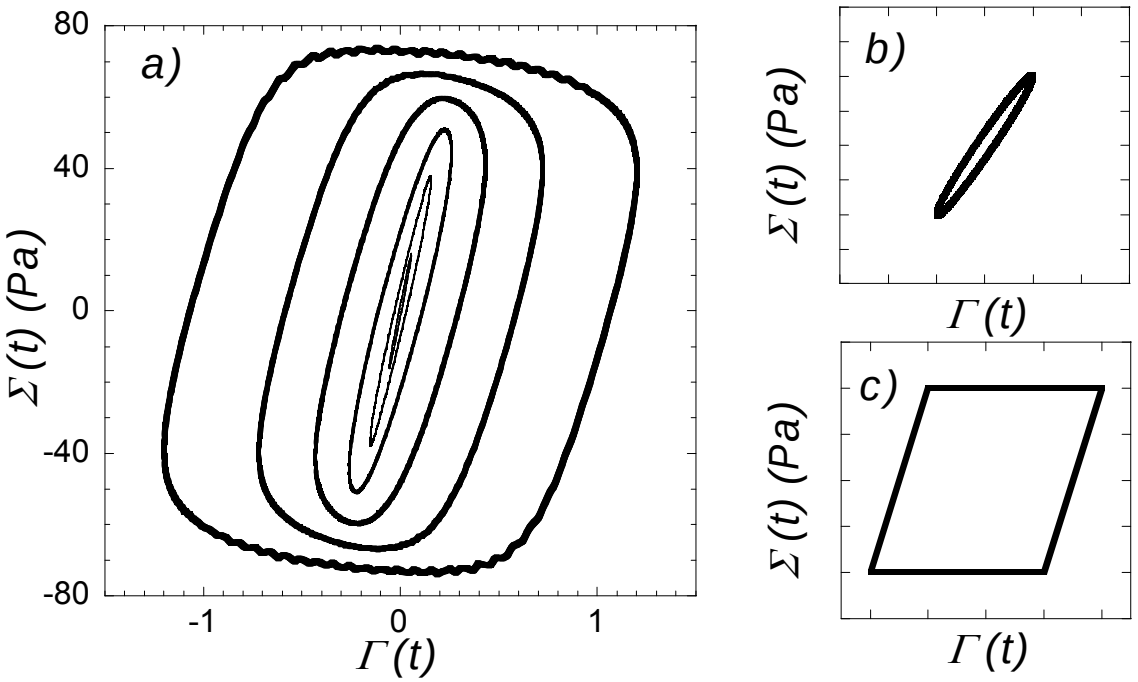

Figure 7 : a) Parametric plots of stress Σ(t) versus strain Γ(t) for applied strain amplitudes $\Gamma_0 = 0.055$, 0.15, 0.25, 0.43, 0.72 and 1.2 corresponding to contours of increasing thicknesses. The frequency is equal to 1 Hz. The sample is Gillette foam (bubble size 28 μm). Figures b) and c) schematically illustrate the response expected for viscoelastic (b) and elastoplastic response (c).

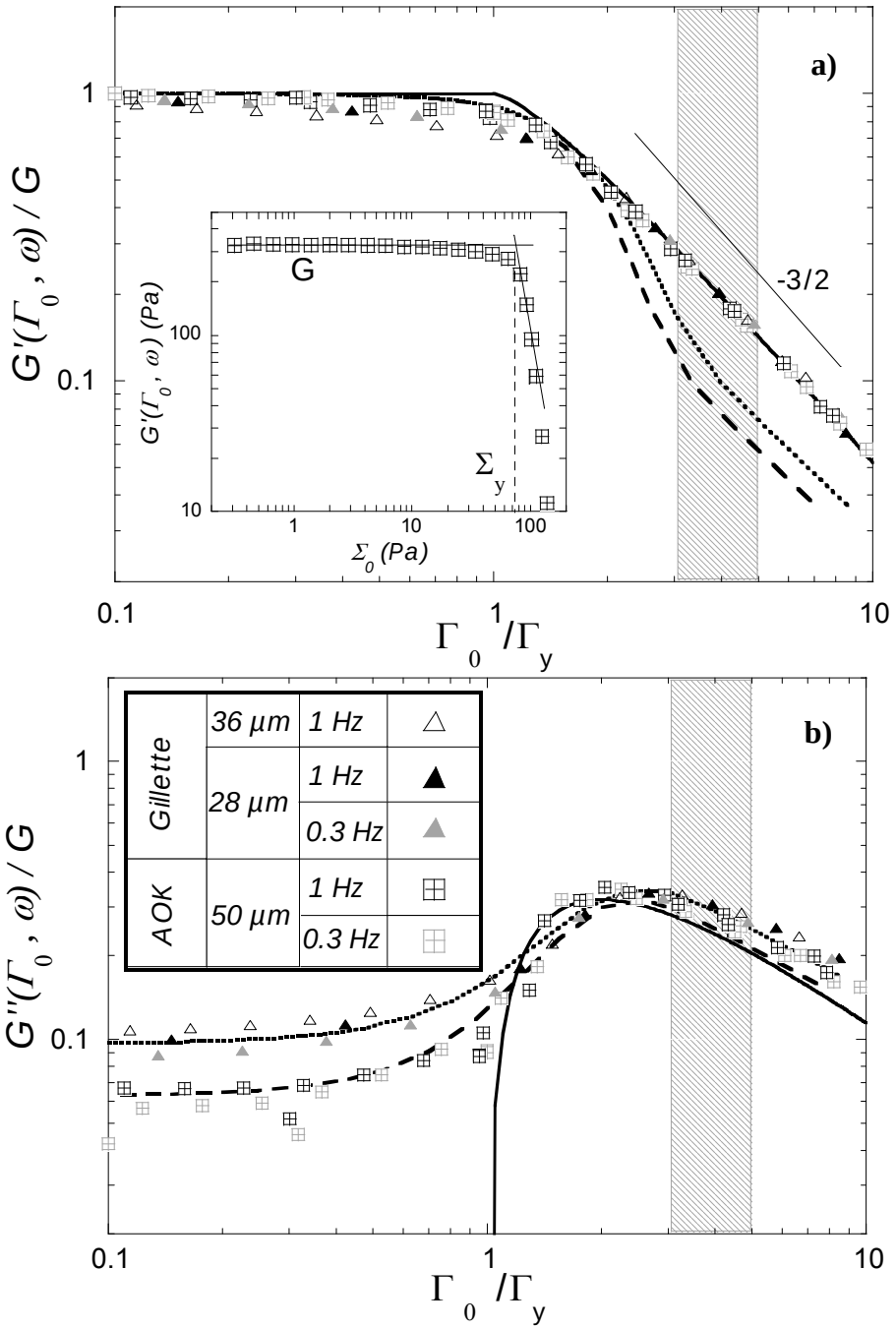

Figure 8: Normalised elastic and loss shear moduli versus normalised strain amplitude. The symbols correspond to Gillette and AOK foams at two frequencies, as shown in the legend of (b). The full line corresponds to the elastoplastic oscillatory response (Eq. (15)). The other lines show the prediction of the SGR model (see text) (dashed line: $x = 1.07$, $\Omega = 0.3$ and $\Gamma_{SGR} = \Gamma_y$, dotted line: $x = 1.05$, $\Omega = 0.3$ and $\Gamma_{SGR} = 0.85\,\Gamma_y$). In the hatched region, the onset of strain localization is observed. The insert in a) shows the evolution of the elastic modulus with stress amplitude for AOK foam.

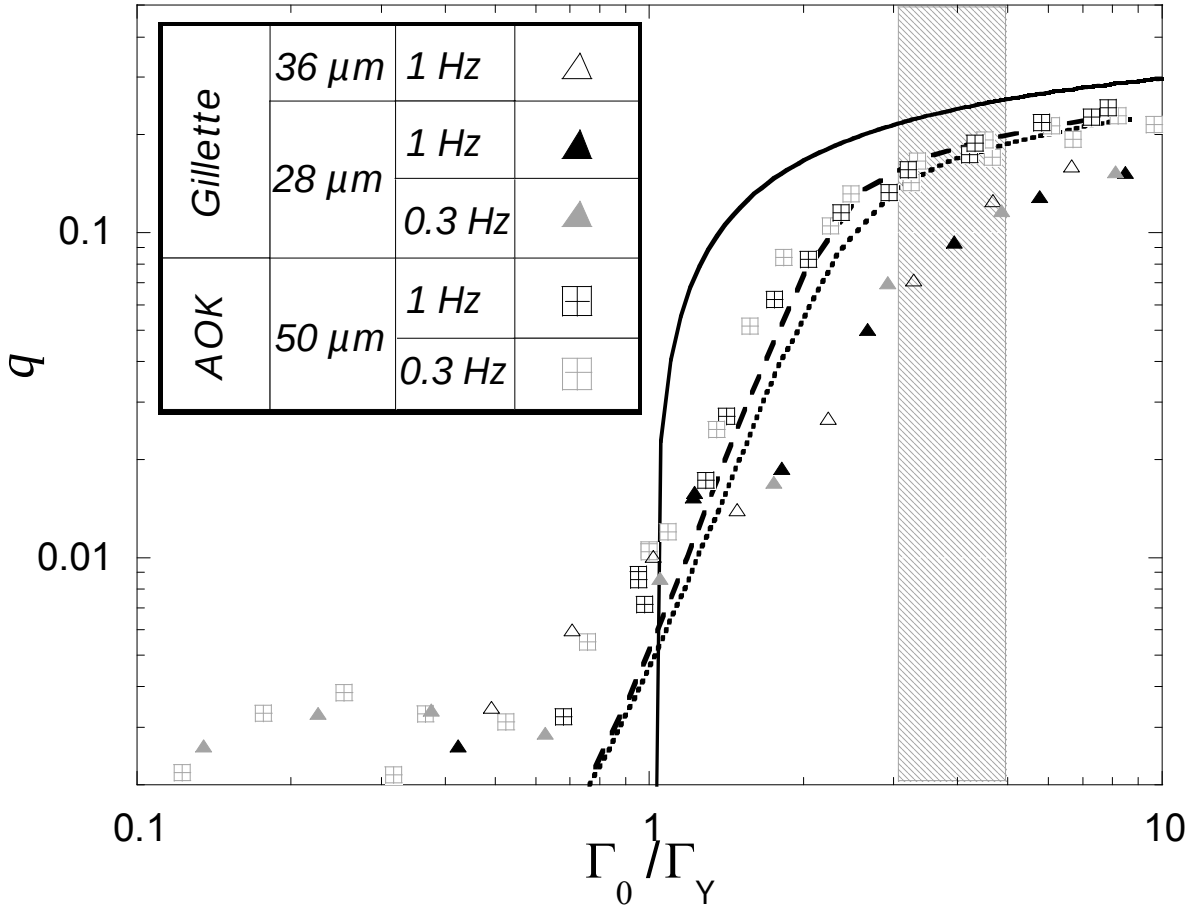

Figure 9 : Stress residual q defined in Eq. **(7)** versus normalised strain amplitude, for Gillette and AOK foams as shown in the legend. The continuous line corresponds to the elastoplastic oscillatory response (Eq. (15)). The other lines correspond to the SGR model (dashed line: x = 1.07, Ω = 0.3 and $\Gamma_{SGR} = \Gamma_y$, dotted line: x = 1.05, Ω = 0.3 and $\Gamma_{SGR} = 0.85\Gamma_y$). In the hatched region, the onset of strain localization is observed.

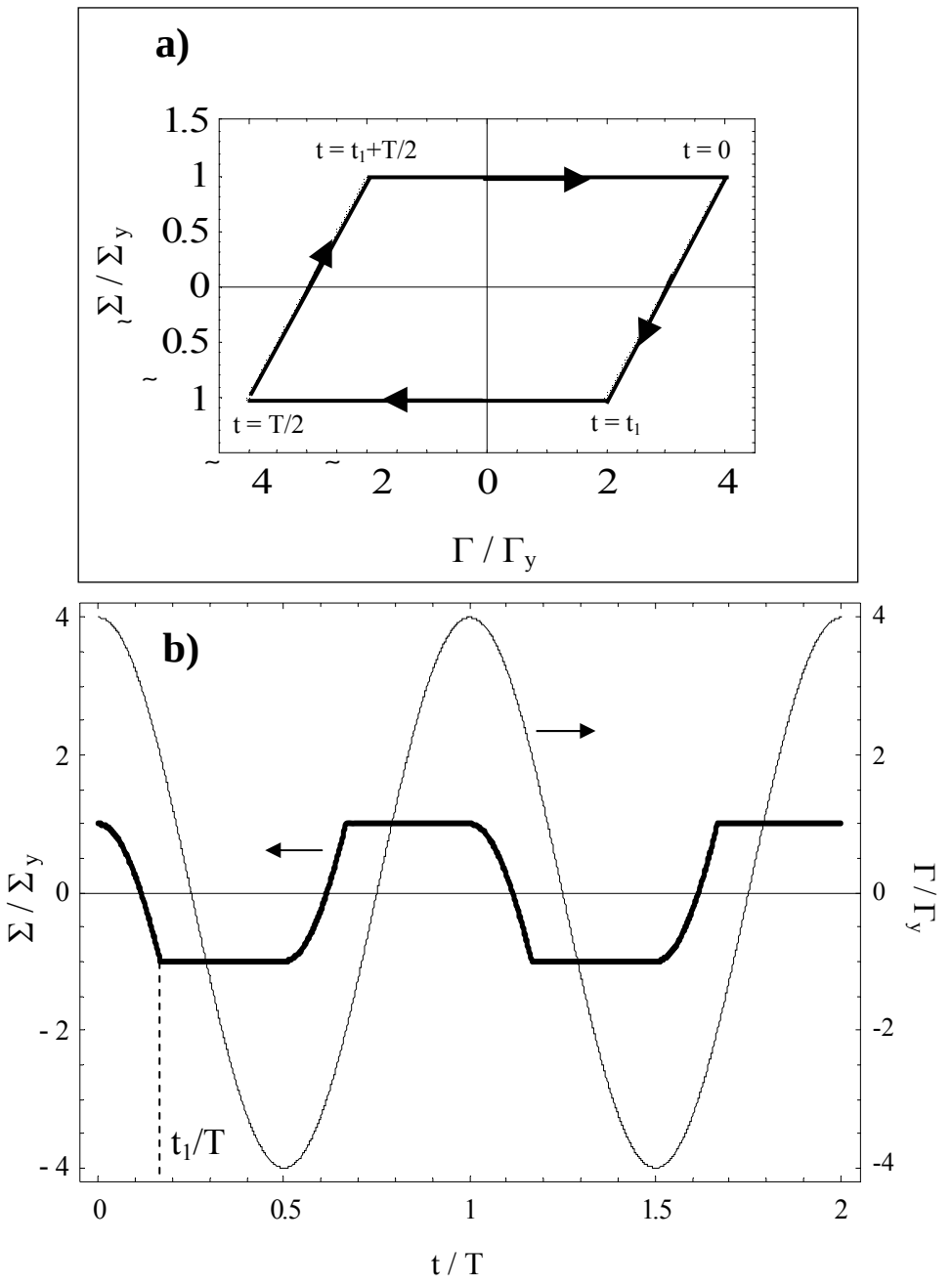

Figure 10 : a) Elastoplastic stress-strain relation, in response to a sinusoidal applied strain of period T and amplitude Γ_0 (cf. Figure 1a). The instant t_1 is defined by Eq. (14). b) Time evolution of the stress (thick line) if a sinusoidal strain (thin line) is imposed with an amplitude exceeding the yield strain.